Dalton Transactions

New Supramolecular Tecton: The Crucial Impact of the Polycation Charge and Geometry of H-Bonds on the Structure and Properties of Halometallates in the Solid State

Journal:	*Dalton Transactions*
Manuscript ID	DT-ART-02-2025-000318.R1
Article Type:	Paper
Date Submitted by the Author:	19-Mar-2025

Complete List of Authors:	Shestimerova, Tatiana; Lomonosov Moscow State University, Chemistry Medved'ko, Alexey; Lomonosov Moscow State University, Chemistry Department; FSBIS N D Zelinsky Institute of Organic Chemistry of the Russian Academy of Sciences, Bykov, Michael; Lomonosov Moscow State University, Department of Chemistry Kalinin, Mikhail ; Lomonosov Moscow State University, Chemistry Metlin, Mikhail; P.N. Lebedev Physical Institute of the Russian Academy of Sciences Taydakov, Ilya; P. N. Lebedev Institute of Physics, Russian Academy of Sciences, Luminescence; FSBIS N D Zelinsky Institute of Organic Chemistry of the Russian Academy of Sciences, Gontcharenko , Victoria ; P.N. Lebedev Physical Institute of the Russian Academy of Sciences Zheng, Wei; University at Albany, Chemistry Dikarev, Evgeny; University at Albany, Chemistry Vatsadze, Sergey; M.V. Lomonosov Moscow State University, Department of Chemistry; FSBIS N D Zelinsky Institute of Organic Chemistry of the Russian Academy of Sciences, Shevelkov, Andrei; Moscow State University, Chemistry

ARTICLE

New Supramolecular Tecton: The Crucial Impact of the Polycation Charge and Geometry of H-Bonds on the Structure and Properties of Halometallates in the Solid State

Received 00th January 20xx,
Accepted 00th January 20xx

DOI: 10.1039/x0xx00000x

Tatiana A. Shestimerova,[a] Aleksei V. Medved'ko,[b] Mikhail A. Bykov,[a] Mikhail A. Kalinin,[a] Mikhail T. Metlin,[c] Ilya V. Taydakov, [b,c] Victoria E. Gontcharenko,[c] Zheng Wei,[d] Evgeny V. Dikarev,[d] Sergey Z. Vatsadze, [a,b] and Andrei V. Shevelkov[a,†]

New tricationic organic supramolecular tecton has been designed and synthesized. Contrary to known mono- and dicationic species, this new molecule, being a "three-way connector", allows assembling infinite supramolecular sheets and nets upon interaction with appropriate inorganic counterpart complex anions. In this work, triprotonated 6-amino-5,7-dimethyl-1,3-diazaadamantane, comprising two secondary and one primary nitrogen atoms, is utilized as a trication to form hybrid compounds with iodometallate anions by exercising five hydrogen bonds at the time. It is shown that the bulky cation works simultaneously as a spacer and a connector, such that the positions of inorganic $[MI_6]^{3-}$ anions (M = Sb, Bi) in the crystal structures are defined by five hydrogen bonds and are well-separated from each other. The latter is considered as a prerequisite for the hybrid compounds to display optical properties originating from the undisturbed electronic structure of individual inorganic anions.

Introduction

Ammonia and amines are very important building blocks in creating supramolecular assemblies *via* hydrogen bonding.[1-3] Depending on the substitution at the N atom of the amine as well as on the degree of its protonation, one can envision several distinct cases (Fig. 1).

Figure 1 clearly shows that increasing the number of R-substituents (alkyl or aryl groups, not carbonyls) decreases the number of possible H-bonds that could be formed by a particular amine or by its protonated form. This leads to a simple conclusion that cases I-III could serve as edges in the potential supramolecular H-bonded architectures, whilst case IV would only result in terminating modes.

Increasing the number of N atoms in a molecule leads to increasing the possible ways for supramolecular architectures formation (Fig. 2).

It was demonstrated recently[4] that combining in one molecule two protonated tertiary nitrogen atoms (1,3-diazaadamantane) led to the creation of a novel bridging supramolecular building block with a general structure of H–N^+(molecule)N^+–H.

These simple considerations bring about the conclusion that an addition of the nitrogen atom (in its protonated form) should increase the dimensionality of the possible H-bonded network (Fig. 3). Clearly, an adamantane derivative with the highest number of nitrogen atoms is urotropine. However, its protonation is limited to one or two nitrogen atoms,[5] because more acidic conditions cause its decomposition. The alternative way to increase the number of H-bonding sites is an addition of an amino-group to 1,3-diazaadamantanes thus increasing the number of nitrogen atoms to three and affording five H-bonds at a time. Such an idea has not been explored prior to this work.

Apparently, the nature of the counter anion also plays a very important role in the formation of a particular supramolecular product. In recent years, halometallate anions have come to the forefront of modern research, first, owing to the discovery of so-called lead-iodine perovskites demonstrating excellent light-harvesting properties with high energy conversion[6-9]. Subsequent broad investigations of other post-transition metal halide complexes have unveiled other important properties including bright luminescence in a wide spectral range observed for many hybrid compounds of Sb^{3+} and Bi^{3+}.[10-16]

[a] *Department of Chemistry, Lomonosov Moscow State University 119991 Moscow, Russia*
[b] *N.D. Zelinsky Institute of Organic Chemistry RAS 119991 Moscow, Russia*
[c] *P.N. Lebedev Physical Institute of the Russian Academy of Sciences 119991 Moscow, Russia*
[d] *Department of Chemistry, University at Albany SUNY, Albany New York 12222, United States*
† Corresponding author shev@inorg.chem.msu.ru

Electronic Supplementary Information (ESI) available: TGA curves, IR spectra, XPD patterns, and crystallographic data for compounds 1 and 2, and luminescent decay fitting parameters for compound 1. See DOI: 10.1039/x0xx00000x

ARTICLE

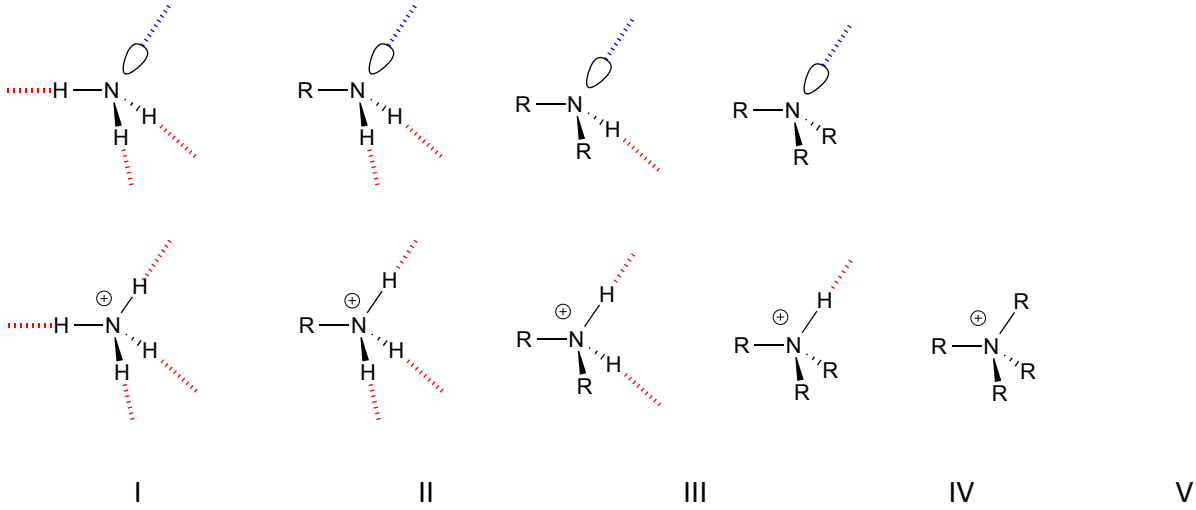

Figure 1. Possible modes of H-bond formation for all monoamines. Upper row – neutral amines, lower row – protonated ammonium cations. Red dotted bond – H-bond donor, blue dotted bond – H-bond acceptor. Quaternary ammonium cation (V) is shown for the completeness of the picture.

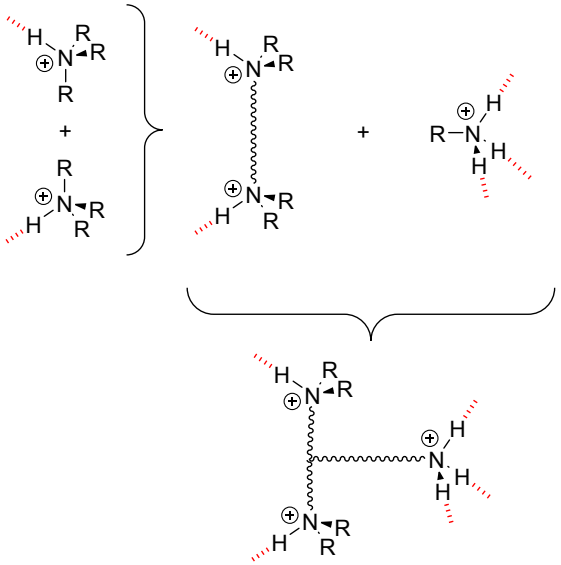

Figure 2. Possible modes of H-bond formation for combination of two tertiary diamines resulting in bridging H-bond manner of the organic ligand. Combination of bis-tertiary diamine with primary amine in the same molecule leads to the three-way connector. Red dotted bond – H-bond donor.

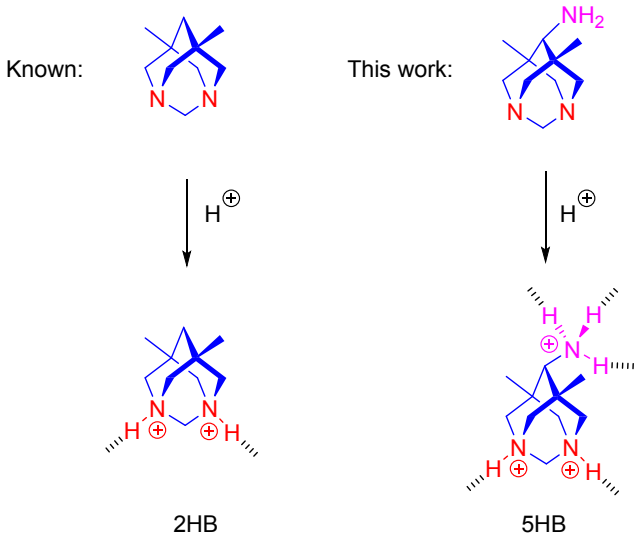

Figure 3. Previously known (left) and new (right) modes of 1,3-diazaadamantane polyammonium building blocks for supramolecular assembly (only the modes with HB donor capacities are shown).

Herein we introduce a new supramolecular tecton, 6-amino-5,7-dimethyl-1,3-diazaadamantane, comprising two secondary and one primary nitrogen atoms, which upon *tris*-protonation could serve as a 3-point connector (Fig. 3) capable of forming up to five H-bonds as an H-bond donor. We describe a facile path to new hybrid compounds of the general formula (3*A*10)(MI$_6$)·3H$_2$O, where 3*A*10 is a 6-amino-5,7-dimethyl-1,3-diazaadamantane cation $[C_{10}N_3H_{22}]^{3+}$ and M = Sb (**1**) or Bi (**2**). We discuss their crystal structures that feature a complete isolation of inorganic $[MI_6]^{3-}$ octahedral anions embedded in a 3-dimensional framework of H-bonds constructed by utilizing all five N–H interactions. Finally, we present optical properties of two new compounds that stem from the undisturbed electronic structures of isolated inorganic anions.

Results and discussion

Compounds **1** and **2** were synthesized by facile reactions of 6-amino-5,7-dimethyl-1,3-diazaadamantane with antimony or bismuth triiodides in aqueous hydroiodic acid. The precipitated and washed off yellow (**1**) and orange (**2**) crystals are stable for weeks when stored in Petri dishes (Fig. S1 of the ESI) and start to decompose upon heating at about 50 °C losing all water at 100 (**1**) and 95 °C (**2**), see Figures S2 and S3 in the ESI.

The compounds are isomorphous and crystallize in the orthorhombic space group *Pnma* (Table S1). The crystal structures consist of three moieties, namely: the triprotonated organic cation, the $[MI_6]^{3-}$ inorganic anion (*M* = Sb or Bi), and solvent water molecules, in the ratio of 1:1:3. The organic cation indeed offered all of its three protonated nitrogen atoms to form five hydrogen bonds of various types (Fig. 4).

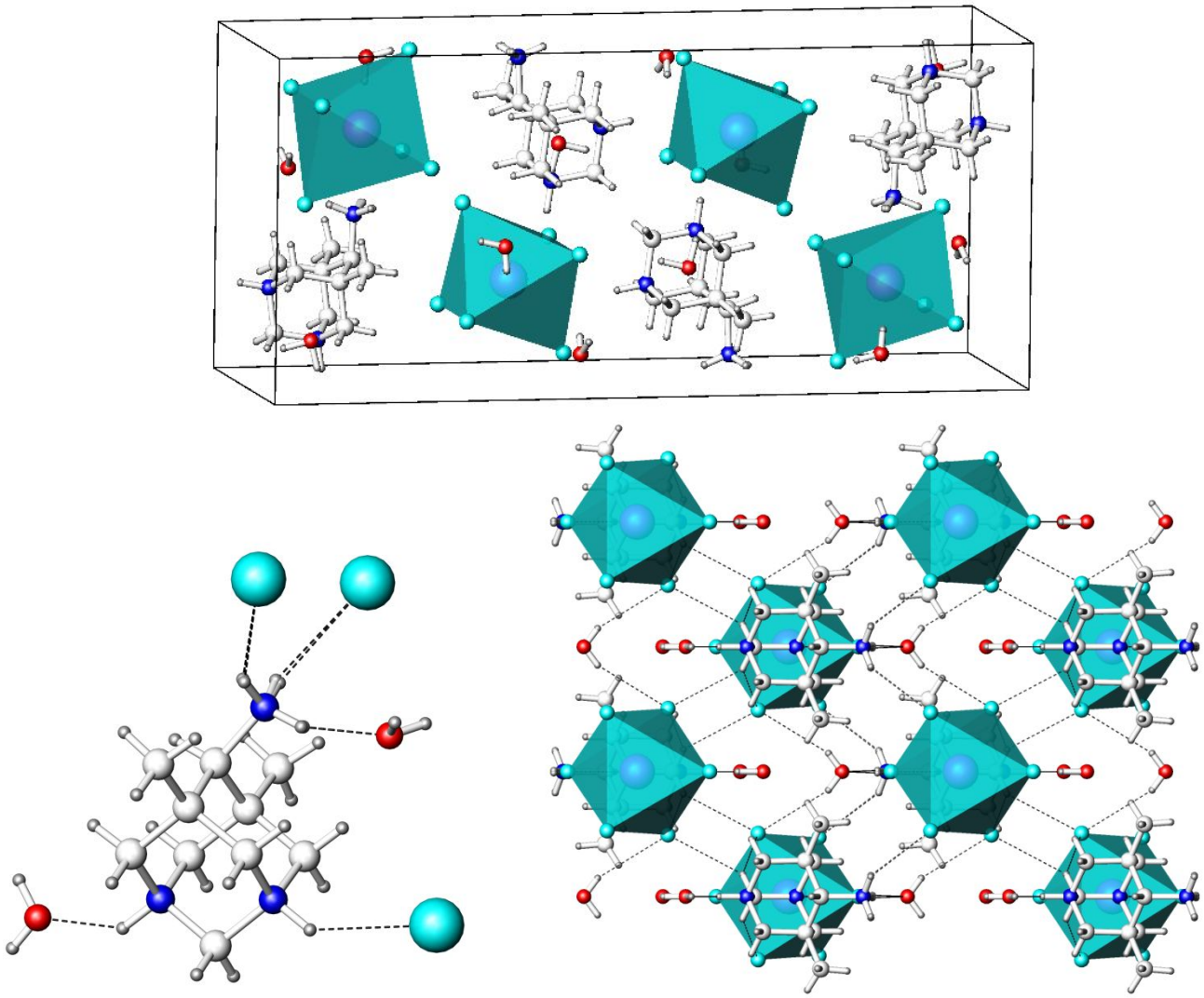

Figure 4. Crystal structure of $3A10(MI_6)\cdot 3H_2O$ ($3A10 = C_{10}N_3H_{22}^{3+}$; M = Sb or Bi); a whole unit cell with three basic structural moieties is depicted (top). The surroundings of the triprotonated 6-amino-5,7-dimethyl-1,3-diazaadamantane with H-bonds (bottom, left) and a projection of the crystal structure onto [100] plane (bottom, right). M atoms are shown in blue, iodine in cyan, oxygen in red, carbon in light grey, and hydrogen in dark grey; dashed lines represent hydrogen bonds.

Surprisingly, the cation's coordination mode is not symmetric: two nitrogen atoms of the diazaadamantane cage show different coordination. One of those forms a N–H···O bond with water oxygen, whereas the other one forms a N–H···I bond with an iodine atom of the inorganic anion. However, the C–N bond lengths for both nitrogen atoms are around 1.50 Å, which points out to an equal positive charge on them.[17,18]

In general, the structural motif of both protonated cage N atoms is virtually identical to that described previously.[5] The third nitrogen atom of the new tecton is also protonated to become an ammonium moiety, which forms three hydrogen bonds: one with water oxygen and two with iodine atoms. Thus, the triply protonated amino-diazadamantane molecule works as an unsymmetric "three-way connector" forming five intermolecular H-bonds.

In both structures, the H···I distances lie in the range of 2.69−2.76 Å, which is slightly shorter than the typical H···I distances of 2.80-2.85 Å.[19-22] We note that the C–H···I hydrogen bonds are also present in the structures, however, the corresponding H···I distances exceed 3 Å, making these bonds approaching the sum of the van der Waals radii of hydrogen and iodine.[23,24] Although compounds **1** and **2** are isomorphous, there are minute differences in the hydrogen bond lengths and the degree of the cage distortion in the cations, which can be traced by minor differences in the IR spectra of two compounds (Fig. S4 of ESI).

The examples of organic cations serving as templates/tectons by forming multifold H-bonds with inorganic anions and/or solvent molecules are plentiful. For instance, deprotonated 1,4-diazacycloheptane, also known as homopiperazinium, utilizes both nitrogen atoms to form a total of four H-bonds, with the nature of an acceptor atom depending on the chemical composition of a compound.[25-28] An example of a triprotonated tecton is provided by recently published N,N,N′,N″,N″-pentamethyldiethylenetriamine, which can be used in three different conformations to form hybrid derivatives with Sb(III) chloride.[29] In them, each nitrogen of the triamine accepts only one hydrogen upon protonation, thus this triamine makes only three hydrogen atoms available for forming H-bonds. In the case of **1** and **2**, one organic cation forms five relatively strong H-bonds, which makes this cation, triprotonated 6-amino-5,7-dimethyl-1,3-diazaadamantane, a unique supramolecular tecton.

The inorganic anions in the crystal structures of **1** and **2** are slightly distorted [MI$_6$] octahedra; the Bi–I distances range from 3.01 to 3.12 Å and those of Sb–I range from 2.94 to 3.08 Å (Table 1). Although the Sb^{3+} cation, unlike its Bi(III) congener, is keen to display its stereo active s^2 lone pair,[30-35] the distortion of the [SbI$_6$] octahedron is modest and does not outplay that of the [BiI$_6$] octahedron, with the deviation of the I–M–I angles not exceeding 6 degrees in both crystal structures.

Table 1. Selected interatomic distances and angles in the MI$_6^{3-}$ anion in the crystal structures of **1** and **2**.

Atoms	Distance, Å	Atoms	Angle, °
1			
Sb1–I2 (×2)	3.0820(3)	I3—Sb1—I4	174.585(12)
Sb1–I3	2.9721(4)	I5—Sb1—I2	178.431(9)
Sb1–I4	3.0481(4)	I5—Sb1—I2	178.429(9)
Sb1–I5 (×2)	2.9373(3)		
2			
Bi1–I2 (×2)	3.1192(6)	I3—Bi1—I4	174.073(18)
Bi1–I3	3.0224(8)	I5—Bi1—I2	178.100(14)
Bi1–I4	3.1095(8)	I5—Bi1—I2	178.101(14)
Bi1–I5 (×2)	3.0079(6)		

The +3 charge of the triprotonated 6-amino-5,7-dimethyl-1,3-diazaadamantane cation matches the −3 charge of the [MI$_6^{3-}$] anions ensuring their 1:1 ratio (and thus a neutrality of a whole compound) in the crystal structure. The organic cations, inorganic anions, and water molecules are linked with the help of hydrogen bonds to form a three-dimensional supramolecular structure, which projection onto the [100] plane is shown in Figure 4. Clearly, the triprotonated cation releases all its nitrogen donor sites to form hydrogen bonds in such a way that the inorganic anions are separated from each other by the cations and water molecules (Table 2). In both crystal structures, the closest distance between iodine atoms of the neighboring [MI$_6$] octahedra is over 4.2 Å, which exceeds twice the van der Waals radius of iodine.[23,24] Therefore, utilization of the triprotonated 6-amino-5,7-dimethyl-1,3-diazaadamantane cation ensures the complete isolation of inorganic anions in the crystal structure and precludes their direct interaction with each other.

Table 2. Hydrogen bonding in the crystal structures of **1** and **2**.

D–H···A	d (D–H), Å	d (H···A), Å	d(D···A), Å	Angle (D–H···A), °
1				
N3–H3A···O2#1	0.87(5)	1.88(5)	2.734(5)	167(5)
N3–H3B···I5#2	0.91(4)	2.70(4)	2.521(3)	150(3)
N3–H3B#3···I5#4	0.91(4)	2.70(4)	2.521(3)	150(3)
N5–H5···O1	0.90(5)	1.95(5)	2.670(5)	136(4)
N4–H4···I4#5	0.77(5)	2.83(5)	3.540(3)	156(5)
O1–H1A···I5#6	0.82(4)	2.98(4)	3.704(3)	149(4)
O1–H1A···I5#7	0.82(4)	2.98(4)	3.704(3)	149(4)
O2–H2#3···I2#7	0.84(4)	2.97(4)	3.732(3)	152(4)
O2–H2···I2#6	0.84(4)	2.97(4)	3.732(3)	152(4)
C10–H10B#3···I2#4	0.99	3.01	3.745(3)	132.3
C10–H10B#3···I2#8	0.99	2.98	3.715(3)	132.3
C10–H10A···I2#5	0.99	2.98	3.715(3)	132.3
C10–H10A···I2#6	0.99	3.01	3.745(3)	132.3
2				
N3–H3A···O2#1	0.81(7)	2.01(8)	2.739(10)	150(10)
N3–H3B···I5#2	0.86(14)	2.77(14)	3.507(3)	145(12)
N3–H3B#3···I5#4	0.86(14)	2.77(14)	3.507(3)	145(12)
N5–H5···O1	0.90(10)	1.90(10)	2.653(9)	140(8)
N4–H4···I4#5	0.79(7)	2.78(8)	3.547(7)	166(9)
O1–H1A···I5#6	0.84(5)	3.12(4)	3.703(5)	128(3)
O1–H1A···I5#7	0.84(5)	3.12(4)	3.703(5)	128(3)
O2–H2#3···I2#7	0.79(4)	3.01(4)	3.732(3)	152(4)
O2–H2···I2#6	0.79(4)	3.01(4)	3.732(3)	152(4)
C10–H10B#3···I2#4	0.99	3.00	3.726(6)	132.5
C10–H10B#3···I2#8	0.99	2.98	3.715(3)	132.3
C10–H10A···I2#5	0.99	2.98	3.715(3)	132.3
C10–H10A···I2#6	0.99	3.00	3.726(6)	132.5

#1 [x, y, 1+z] #2 [½-x, ½+y, ½+z] #3 [x, ½-y, z] #4 [½-x, -y, ½+z] #5 [½+x, ½-y, $^3/_2$-z] #6 [½-x, ½+y, -½+z] 7# [½-x, -y, -½+z] #8 [[½+x, y, $^3/_2$-z]

It is expected that in the absence of direct interactions between the inorganic [MI$_6$]$^{3-}$ anions, the band structure will be dominated by flat bands; therefore, band gaps of 2.1−2.6 eV should be anticipated since the charge transfer proceeds from the 5p states of iodine atoms at the top of a valence band to the 5p (6p) states of antimony (bismuth) atoms at the bottom of a conduction band.[36-38] Indeed, the analysis of the optical diffuse reflectance measured for both samples and converted into absorbance data by the Kubelka-Munk method led to the values

of 2.5 (**1**) and 2.2 (**2**) eV, in accordance with yellow (**1**) and orange (**2**) colors of compounds, respectively (Fig. 5).

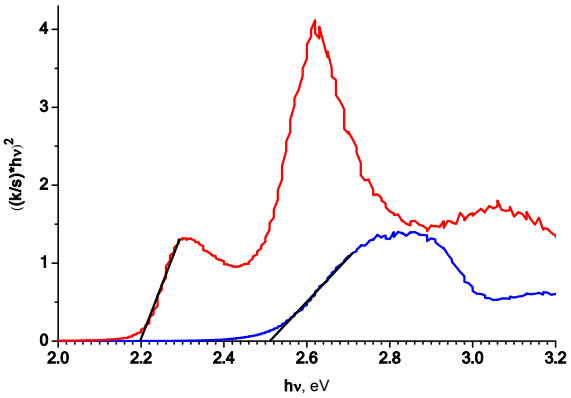

Figure 5. Kubelka-Munk plots for **1** (blue) and **2** (red).

Although rather strong hydrogen bonds may contribute to the band structure near the respective Fermi levels for both compounds, such a contribution should be vanishingly small in **1** and **2** because the H···O and H···I distances are not short enough (Table 2) compared with those that are capable of affecting the band gap by slightly pushing the 5*p* states of iodine atoms to higher energy.[5,20] Therefore, the observed band gaps can be attributed to the charge transfer in the pristine $[MI_6]^{3-}$ anions.

Figure 6 shows the photoluminescence (PL) spectra for both compounds. Whereas **1** displays bright PL at 77 K with an exciton lifetime of 45 μs (see Table S2 in SI), the PL signal for compound **2** is rather weak. The emission maxima are observed at 724 nm for **1** and 753 nm for **2**, which means that the emission bands shift towards the near-IR region. Indeed, when irradiated by a 365 nm laser beam at 77 K, compound **1** displays a bright red glow owing to the width of the spectral line protruding to the visible part of the spectrum. For compound **2** such glowing is hardly observed mainly due to lower intensity of PL but also because of a greater shift towards the IR region.

For both compounds, PL spectra are characterized by large Stocks shifts, 1.0 eV for **1** and *ca.* 2.4 eV for **2**, as well as by wide spectral bands with full-width half-maximum (*FWHM*) of about 125 nm for both compounds (Fig. 6). Given that isolated positions of the $[MI_6]$ octahedra make collective excitations least probable, we attribute excitation to the metal-centered transitions that involve ns^2 lone pairs on Sb^{3+} and Bi^{3+} cations. Excitation leads to the population of the respective *np*-states, and the distortion of the $[MI_6]$ octahedra induces small polarons capable of trapping charge carriers leading to self-trapped excitons.[31,39,40] The distortion of $[MI_6]$ octahedra is facilitated by the absence of outer covalent bonds, which explains large Stocks shifts and a broadband character of PL emission.

A comparison of the PL properties of **1** and **2** with other iodoantimonates and iodobismuthates cannot be straightforward, because in the latter compounds the $[MI_6]$ octahedra are joined into dimers or trimers. However, they also display PL emission in the red or near-IR region due to self-trapped excitons. The emission is characterized by narrower bands and relatively small Stocks shifts of 0.5-0.9 eV.[12,41-43] Most likely, these properties can be attributed to less distorted iodometallate anions and their smaller spatial separation in the crystal structure.

Experimental

Synthetic procedures. For the synthesis of target compounds, 6-amino-5,7-dimethyl-1,3-diazaadamantane was first obtained according to a published procedure.[44] BiI_3 (99.99 %), SbI_3 (99 %) P_{red} (98 %), $H_2O_{(dist)}$, and I_2 (99.99 %) were also used as starting reagents. Hydroiodic acid (stabilized) was synthesized by hydrolysis of freshly prepared PI_3 as described in detail elsewhere.[45] The HI acid (stabilized) was distilled at 126 °C.

For the preparation of **1**, 6-amino-5,7-dimethyl-1,3-diazaadamantane (79 mg, 0.44 mmol) and antimony triiodide (221 mg, 0.44 mmol) were separately dissolved in 2 mL of hydroiodic (20 %) acid and then two solutions were mixed, which immediately resulted in precipitation of the yellow powder of **1**.

The orange powder of the compound **2** was prepared by the same procedure using 6-amino-5,7-dimethyl-1,3-diazaadamantane (70 mg, 0.40 mmol) and bismuth triiodide (230 mg, 0.40 mmol).

For the crystal growth of **1** and **2**, the same synthetic procedure as for the powder samples preparation was used but with 10 mL of 20% hydrochloric acid. The solutions obtained after mixing the reagents were left for 1 week to form polycrystalline precipitates. Single crystals suitable for structure determination and property measurements were separated by filtration and dried at room temperature.

Thermal analysis. Thermogravimetric analysis was performed using a NETZSCH 209 F1 Libra thermobalance. Calibration was performed with $CaC_2O_4{\cdot}2H_2O$ in order to increase the accuracy of mass detection. The sample was heated in an alumina crucible under dry nitrogen flow up to 350 °C with the ramp rate of 10 °C·min^{-1}. The NETZSCH Proteus Thermal Analysis program was used for data processing.

Powder X-ray diffraction analysis (PXRD) was performed on the Imaging Plate Guinier Camera (Huber G670, Cu-$K_{\alpha 1}$ radiation, λ = 1.540598 Å) with the 2θ angles ranging from 3 to 100° with a 0.005° increment. The data were collected by scanning the image plate four times with an exposure time of 1200 s at room temperature. For measurement, the microcrystals or powders were finely crushed in an agate mortar, and the resulting fine powder was fixed on a holder. The experimental patterns, presented in the ESI (Figures S5 and S6) show excellent match with the pattern calculated from the crystal data. Additionally, Rietveld refinement was performed against the powder XRD data and yielded the crystal data matching those obtained from the single crystal structure refinement (ESI, Figure S7 and Table S3)

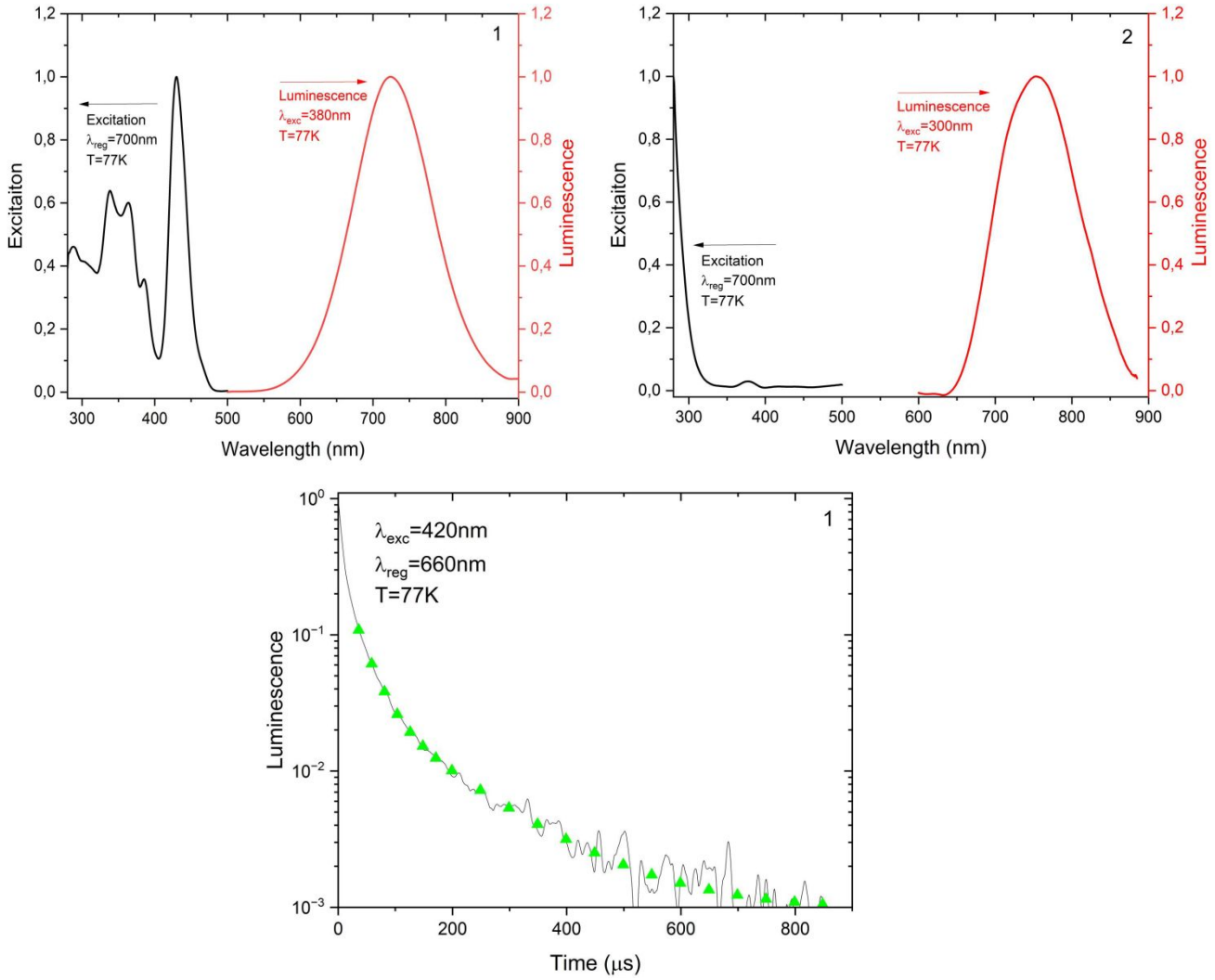

Figure 6. PL spectra of **1** (left), **2** (right), and PL lifetime for **1** (bottom).

Crystal structure determination. Single crystal X-ray diffraction studies of a suitable crystal of **1** were carried out on a Bruker D8 Quest diffractometers equipped with a CMOS detector (MoK_α, λ = 0.71073 Å, graphite monochromator).[46] Data were corrected for absorption effects using the numerical methods from crystal shape implemented in SADABS (2016/2).[47] The crystal structure was solved by the intrinsic phase methods using the Olex2,[48] which gave positions of iodine and antimony atoms. Difference Fourier syntheses in Shelxt (SHELXL-2018/3) gave the positions of nitrogen, and carbon atoms of the cations, and oxygen atoms of water molecules.[49] The hydrogen atoms were initially refined using the riding model. In the final stage of the refinement, hydrogens attached to nitrogen atoms were allowed to refine freely with their atomic displacement parameters set as 1.3 of the parent nitrogen atoms. The crystal structure was refined in anisotropic approximations of atomic displacement parameters for all atoms except hydrogens.

Single crystals of **2** were selected directly from the reaction products. The single crystal diffraction data were measured at 100(2) K on a Bruker D8 VENTURE with PHOTON 100 CMOS detector system and graphite monochromator equipped with a Mo-target X-ray tube. A frame width of 0.50° and an exposure time of 15 s/frame were employed for the data collection. Data reduction and integration were performed with the Bruker software package SAINT (Version 8.38A).[47] Data were corrected for absorption effects using the semi-empirical methods (multi-scan) as implemented in SADABS (Version 2014/5).[47] The crystal structure was solved by direct methods using the SHELXTL (Version 2018/3) program package,[49] which gave positions of bismuth and iodine atoms. Difference Fourier syntheses gave the positions of nitrogen and carbon atoms of cations and oxygens of water molecules. Hydrogen atoms were calculated and further refined using the riding model. In the final step, the crystal structure was refined with anisotropic approximations of atomic displacement parameters for all non-hydrogen atoms.

Selected bond distances and H-bonds parameters are given in Tables 1 and 2 for compounds **1** and **2**, whereas crystal data are presented in Table S1 (ESI). Figure S8 of the ESI displays the surrounding of the cations.

Optical Spectroscopy. Optical diffuse reflectance spectra were recorded using a Perkin-Elmer Lambda 950 UV-viz spectrometer with an attached diffuse reflectance accessory. Measurements were performed at 298 K in the spectral range of 250–1200 nm, with the scanning rate of 2 nm·s^{-1} using finely ground polycrystalline samples. The data were processed using the Kubelka-Munk theory approximation and linearized in the $[(k/s)\cdot h\nu]^{1/2} - (h\nu)$ coordinates with $h\nu$ along the x axis and $[(k/s)\cdot h\nu]^{1/2}$ along the y axis, where k is the absorption coefficient, s is the scattering coefficient, and h is the Planck constant.[50] The k/s relation known as a remission function was calculated according to the literature as $k/s = (1-R)^2/2R$, where R is the absolute diffuse reflectance.[51] Extrapolation to $k = 0$ gives an approximate value of the optical E_g of the material.
Photoluminescence excitation and emission steady-state spectra were recorded at room temperature and 77 K with a Horiba-Jobin-Yvon Fluorolog-QM spectrofluorimeter equipped with a 75 W ArcTune xenon lamp and a Hamamatsu R13456 photomultiplier sensitive in the 200-980 nm emission range. For the low-temperature measurements samples were placed in a quartz optical cryostat filled by liquid N_2. Luminescence decays were acquired on the same instrument using pulsed DeltaLed excitation source (λ = 370 nm) and EZ-time software for data analysis.

Conclusions

In summary, we have presented triprotonated 6-amino-5,7-dimethyl-1,3-diazaadamantane as a new supramolecular tecton for constructing organic-inorganic hybrid compounds by utilizing the ability of organic cation to form five hydrogen bonds at a time. Taking new compounds **1** and **2** as examples, we have shown that complete protonation of three nitrogen atoms of 6-amino-5,7-dimethyl-1,3-diazaadamantane ensures formation of the N-H···I and N-H···O bonds with iodine atoms of the $[MI_6^{3-}]$ (M = Sb for **1** and Bi for **2**) inorganic anions and oxygen atoms of solvent water molecules, respectively. The geometry of the cation, in particular, the positions and orientations of nitrogen atoms and respective N–H bonds, lead to the complete isolation of the inorganic anions, with the I···I contacts exceeding twice the van der Waals radius of iodine. As a result, the inorganic anions display properties governed by their pristine electronic structure. They demonstrate band gaps of 2.5 (**1**) and 2.2 (**2**) eV reflecting charge transfer from the *ns* states at the top of the valence band to the *np* states at the bottom of the conduction band as well as near-IR wide-band PL emission due to self-trapped excitons facilitated by local distortions of the octahedral anions devoid of outer covalent bonds.
Therefore, we have developed a new supramolecular tecton, which bulky structure with three nitrogen atoms ensures embedment of MI_6^{3-} anions in such a way that the latter are distributed in an ordered fashion and are well-separated from each other. At the same time, the 3D supramolecular framework made of hydrogen bonds supports perfect ordering of the entire supramolecular assembly. We believe that utilizing bulky triprotonated 6-amino-5,7-dimethyl-1,3-diazaadamantane as a 3-point connector opens the possibility to engineer hybrid compounds formed as a result of embedding isolated inorganic anions into a 3-dimensional network of H-bonds. Moreover, we envisage the possibility of constructing organic-inorganic hybrids by combining inorganic anions of different nature, which will give rise to compounds with properties stemming from the respective anions, whereas triprotonated 6-amino-5,7-dimethyl-1,3-diazaadamantane will ensure formation of a 3D network by forming five H-bonds with inorganic anions.

Author contributions

Conceptualization: T.A.S., S.Z.V. and A.V.S.; data curation: T.A.S., I.V.T., and E.V.D.; methodology: T.A.S. and A.V.M.; formal analysis: A.V.B., V.M.K., Z.W. and M.T.M.; investigation: T.A.S., A.V.M., M.A.B., M.T.M., V.E.G., Z.W. and M.A.K.; writing—original draft preparation: T.A.S., S.Z.V., E.V.D. and A.V.S.; writing—review and editing: T.A.S., I.V.T., E.V.D., S.Z.V. and A.V.S.; supervision: A.V.S.; project administration: A.V.S.; funding acquisition: A.V.S. All authors have read and agreed to the published version of the manuscript.

Conflicts of interest

There are no conflicts to declare.

Data availability

CCDC 2346041 (for 1), and 2363792 (for 2) contains the supplementary crystallographic data for this paper. These data can be obtained free of charge from The Cambridge Crystallographic Data Centre via www.ccdc.cam.ac.uk/structures. Thermal analysis data, IR spectra, cations' surrounding (including bonds lengths), and luminescence decay fitting parameters for compounds 1 and 2 are given in PDF format.

Acknowledgements

The authors are grateful to the Lomonosov MSU Program of Development for providing access to the Bruker D8 QUEST X-ray single crystal diffractometer and NETZSCH 209 F1 Libra thermobalance. This work was supported by the state program # AAAA-A21-121011590082-2. EVD thanks the National Science Foundation (CHE-2400091) for support. The acknowledgements come at the end of an article after the conclusions and before the notes and references.

References

1 L. J. Prins, D. N. Reinhoudt, P. Timmerman, Noncovalent Synthesis Using Hydrogen Bonding, *Angew. Chem. Int. Ed.*, 2001, **40(13)**, 2382.
2 C.-Y. Shi, Q. Zhang, B.-S. Wang, D.-D. He, H. Tian, D.-H. Qu, Highly Ordered Supramolecular Assembled Networks Tailored

by Bioinspired H-Bonding Confinement for Recyclable Ion-Transport Materials, *CCS Chem.,* 2023, **5(6)**, 1422.

3 X. Li, W. Ge, S. Guo, J. Bai, W. Hong, Characterization and Application of Supramolecular Junctions, *Angew. Chem.,* 2023, **135(13)**, e202216819.

4 A. Mezentsev-Cherkes, T. A. Shestimerova, A. V. Medved'ko, M. A. Kalinin, A. N. Kuznetsov, Z. Wei, E. V. Dikarev, S. Z. Vatsadze, A. V. Shevelkov, Synthesis and Supramolecular Organization of the Iodide and Triiodides of a Polycyclic Adamantane-Based Diammonium Cation: The Effects of Hydrogen Bonds and Weak I···I Interactions, *CrystEngComm,* 2021, **23(12**), 2324.

5 T. A. Shestimerova, A. V. Mironov, M. A. Bykov, E. D. Starichenkova, A. N. Kuznetsov, A. V. Grigorieva, A. V. Shevelkov, Reversal Topotactic Removal of Acetone from $(HMTH)_2BiI_5\cdot(CH_3)_2C{=}O$ Accompanied by Rearrangement of Weak Bonds, from 1D to 3D Patterns, *Cryst. Growth Des.,* 2020, **20(1)**, 87.

6 Z. Zhu, C. Chueh, N. Li, C. Mao, A. K.-Y. Jen, Realizing Efficient Lead-Free Formamidinium Tin Triiodide Perovskite Solar Cells via a Sequential Deposition Route, *Adv. Mater.* 2018, **30(6)**.

7 W. L. Leong, Z.-E. Ooi, D. Sabba, C. Yi, S. M. Zakeeruddin, M. Graetzel, J. M Gordon, E. A. Katz, N. Mathews, Identifying Fundamental Limitations in Halide Perovskite Solar Cells, *Adv. Mat.,* 2016, **28(12)**, 2439.

8 S. Kazim, M. K. Nazeeruddin, M. Grätzel, S. Ahmad, Perovskite as Light Harvester: A Game Changer in Photovoltaics, *Angew. Chem. Int. Ed.,* 2014, **53(11)**, 2812.

9 C. Hou, X. Liu, C. Wan, B. Li, T. Lu, C. Ge, Y. Song, A. Wang, Y. Kang, Q. Dong, Designing Guanidine-Based Antimony Halides Luminescence Perovskite Crystals toward Near-Unity Quantum Yield, *Chem. Mat.,* 2023, **35(24)**, 10635.

10 H. Liu, T. B. Shonde, F. Gonzalez, O. J. Olasupo, S. Lee, D. Luong, X. Lin, J. S. R. Vellore Winfred, E. Lochner, I. Fatima, K. Hanson, B. Ma, Efficient Red Light Emitting Diodes Based on a Zero-Dimensional Organic Antimony Halide Hybrid, *Adv. Mat.,* 2023, **35(9)**, 2209417.

11 C. Sun, Z. Deng, Z. Li, Z. Chen, X. Zhang, J. Chen, H. Lu, P. Canepa, R. Chen, L. Mao, Achieving Near-Unity Photoluminescence Quantum Yields in Organic-Inorganic Hybrid Antimony(III) Chlorides with the $[SbCl_5]$ Geometry, *Angew. Chem. Int. Ed.,* 2023, **62(10)**, e202216720.

12 T. A. Shestimerova, N. A. Yelavik, A. V. Mironov, A. N. Kuznetsov, M. A. Bykov, A. V. Grigorieva, V. V. Utochnikova, L. S. Lepnev, A. V. Shevelkov, From Isolated Anions to Polymer Structures through Linking with I_2: Synthesis, Structure, and Properties of Two Complex Bismuth(III) Iodine Iodides, *Inorg. Chem.,* 2018, **57(7)**, 4077.

13 K. M. McCall, C. C. Stoumpos, S. S. Kostina, M. G. Kanatzidis, B. W. Wessels, Strong Electron-Phonon Coupling and Self-Trapped Excitons in the Defect Halide Perovskites $A_3M_2I_9$ (A = Cs, Rb; M = Bi, Sb) , *Chem. Mat.,* 2017, **29(9)**, 4129.

14 K. Kundu, P. Acharyya, K. Maji, R. Sasmal, S. S. Agasti, K. Biswas, Synthesis and Localized Photoluminescence Blinking of Lead-Free 2D Nanostructures of $Cs_3Bi_2I_6Cl_3$ Perovskite, *Angew. Chem. Int. Ed.,* 2020, **59(31)**, 13093.

15 J.-F. Liao, Z. Zhang, L. Zhou, Z. Tang, G. Xing, Achieving Near-Unity Red Light Photoluminescence in Antimony Halide Crystals via Polyhedron Regulation, *Angew. Chem. Int. Ed.,* 2024, **63(24)**, e202404100.

16 A. V. Bykov, T. A. Shestimerova, M. A. Bykov, V. E. Gontcharenko, K. A. Lyssenko, M. T. Metlin, I. V. Taydakov, A. V. Grigorieva, A. V. Shevelkov, Photoluminescent chain-of-dimer anion in a novel hybrid halometallate $(C_5H_{14}N_2)_3\{Sb_2Br_9\}_2$: atypical behavior in one-dimensional anionic systems, *Dalton Trans.*, 2025, **54(4)**, 1541.

17 H. Cui, R. Goddard, K. R. Pörschke, Degradation of Dichloromethane by Bispidine, *J. Phys. Org. Chem.,* 2012, **25(10)**, 814.

18 M. A. Kalinin, A. V. Medved'Ko, M. E. Minyaev, S. Z. Vatsadze, Synthesis of N, N'-Unsymmetrical 9-Amino-5,7-Dimethyl-Bispidines, *J. Org. Chem.,* 2023, **88(11)**, 814.

19 T. Li, Y. Hu, C. A. Morrison, W. Wu, H. Han, N. Robertson, Lead-Free Pseudo-Three-Dimensional Organic–Inorganic Iodobismuthates for Photovoltaic Applications, *Sustain. Energy Fuels,* 2017, **1(2)**, 308.

20 T. A. Shestimerova, M. A. Bykov, Z. Wei, E. V. Dikarev, A. V. Shevelkov, Crystal Structure and Two-Level Supramolecular Organization of Glycinium Triiodide, *Russ. Chem. Bull.,* 2019, **68(8)**, 1520.

21 C. Hrizi, A. Trigui, Y. Abid, N. Chniba-Boudjada, P. Bordet, S. Chaabouni, α- to β-$[C_6H_4(NH_3)_2]_2Bi_2I_{10}$ reversible solid-state transition, thermochromic and optical studies in the p-phenylenediamine-based iodobismuthate(III) material, *J. Solid State Chem.,* 2011, **184(12)**, 3336.

22 O. V. Nesterova, S. R. Petrusenko, V. V. Dyakonenko, O. V. Shishkin, W. Linert, A three-dimensional framework of bis[tris(ethylenediamine)zinc] tetraiodocadmate diiodide assisted by N-H···I hydrogen bonds, *Acta Crystallogr. C,* 2006, **62**, 281.

23 S. Alvarez, A Cartography of the van Der Waals Territories, *Dalton Trans.,* 2013, **42(24)**, 8617.

24 I. Y. Chernyshov, I. V. Ananyev, E. A. Pidko, Revisiting van Der Waals Radii: From Comprehensive Structural Analysis to Knowledge-Based Classification of Interatomic Contacts, *ChemPhysChem,* 2020, **21(5)**, 307.

25 T. A. Shestimerova, A. V. Mironov, M. A. Bykov, A. V. Grigorieva, Z. Wei, E. V. Dikarev, A.V. Shevelkov, Assembling Polyiodides and Iodobismuthates Using a Template Effect of a Cyclic Diammonium Cation and Formation of a Low-Gap Hybrid Iodobismuthate with High Thermal Stability, *Molecules,* 2020, **25(12)**, 2765.

26 A. V. Bykov, T. A. Shestimerova, M. A. Bykov, K. A. Lyssenko, V. M. Korshunov, M. T. Metlin, I. V. Taydakov, A. V. Shevelkov, Molecular and Supramolecular Structure of a New Luminescent Hybrid Compound: $(C_5N_2H_{14})_2[BiBr_6]Br\cdot H_2O$, *Inorganics,* 2022, **10(11)**, 181.

27 A. V. Bykov, T. A. Shestimerova, M. A. Bykov, E. V. Belova, V. E. Goncharenko, P. V. Dorovatovskii, V. N. Khrustalev, A. V. Shevelkov, New Lead-Free Hybrid Halometallates with Dioctahedral Anions Synthesized Using the Template Function of Homopiperazine. *Russ. Chem. Bull.,* 2023, **72(1)**, 161.

28 A. V. Bykov, T. A. Shestimerova, M. A. Bykov, L. A. Osminkina, A. N. Kuznetsov, V. E. Gontcharenko, A. V. Shevelkov, Synthesis, Crystal, and Electronic Structure of $(HpipeH_2)_2[Sb_2I_{10}](I_2)$, with I_2 Molecules Linking Sb_2X_{10} Dimers into a Polymeric Anion: A Strategy for Optimizing a Hybrid Compound's Band Gap, *Int. J. Mol. Sci.,* 2023, **24(3)**, 2201.

29 X. Wen, J. Cheng, P. Qian, Z. Zhang, H. Zeng, L. Huang, G. Zou and Z. Lin, Synthesis and structure-dependent optical properties of two new organic–inorganic hybrid antimony(III) chlorides, *Dalton Trans.*, 2024, **53(1)**, 260.

30 B. Li, J. Jin, M. Yin, X. Zhang, M. S. Molokeev, Z. Xia, Y. Xu, Sequential and Reversible Phase Transformations in Zero-Dimensional Organic-Inorganic Hybrid Sb-Based Halides towards Multiple Emissions, *Angew. Chem. Int. Ed.,* 2022, **61(49)**, e202208881.

31 A. N. Usoltsev, T. S. Sukhikh, A. S. Novikov, V. R. Shayapov, D. P. Pishchur, I. V. Korolkov, I. F. Sakhapov, V. P. Fedin, M. N. Sokolov, S. A. Adonin, Unexpected Polymorphism in Bromoantimonate(III) Complexes and Its Effect on Optical Properties, *Inorg. Chem.,* 2021, **60(4)**, 17837.

32 Y. C. Peng, J. C. Jin, Q. Gu, Y. Dong, Z. Z. Zhang, T. H. Zhuang, L. K. Gong, W. Ma, Z. P. Wang, K. Z. Du, X. Y. Huang,

Unexpected Polymorphism in Bromoantimonate(III) Complexes and Its Effect on Optical Properties, *Inorg. Chem.,* 2021, **60(23)**, 2797.
33 J. R. Sorg, T. Schneider, L. Wohlfarth, T. C. Schäfer, A. Sedykh, K. Müller-Buschbaum, Sb- and Bi-Based Coordination Polymers with N-Donor Ligands with and without Lone-Pair Effects and Their Photoluminescence Properties, *Dalton Trans.,* 2020, **49(15)**, 4904.
34 N. Dehnhardt, A. Böth, J. Heine, Surprising Discoveries on the Way to an Old Compound: Four Transient Iodido Antimonates, *Dalton Trans.,* 2019, **48(16)**, 5222.
35 D. Chen, Z. Song, C. Yang, Y. Wei, G. Liu, L. Meng, Q. Wu, Y. Dang, Nonlinear Optical Effects of Hybrid Antimony(III) Halides Induced by Stereoactive $5s^2$ Lone Pairs and Trimethylammonium Cations, *Inorg. Chem.,* 2024, **63(22)**, 10304.
36 F. Lin, C. Yang, R. Chen, W. Wei, M. Liu, J. Wang, F. Guo, Near-Unity Emission in Zero-Dimensional Sb(III)-Based Halides Intervened by Hydrogen Bonds towards Efficient Solid-State Lighting Technology, *J. Alloys Compd.,* 2024, **976**, 173054.
37 W. Li, Y. Wang, H. Yin, J. Chen, K. Han, F. Liu, R. Zhang, Excitation-Dependent Emission in Sb^{3+}-Doped All-Inorganic Rare-Earth Double Perovskites for Anticounterfeiting Applications, *Inorg. Chem*., 2024, **63(23)**, 10481.
38 Z. P. Zhang, Q. Y. Feng, Y. L. Wei, Z. Y. Gao, Z. W. Wang, Y. M. Wang, Three Iodobismuthates Hybrids Displaying Mono-Nuclear, Dimer and 1-D Arrangements Templated by 1,4-Diazabicyclo[2.2.2]Octane Derivatives: Semiconductor and Photocurrent Response Properties, *J. Clust. Sc.,* 2018, **29(4)**, 725.
39 V. Morad, S. Yakunin, B. M. Benin, Y. Shynkarenko, M. J. Grotevent, I. Shorubalko, S. C. Boehme, M. V. Kovalenko, Hybrid 0D Antimony Halides as Air-Stable Luminophores for High-Spatial-Resolution Remote Thermography, *Adv. Mat.,* 2021, **33(9)**, 2007355.
40 D. Y. Li, J. H. Song, Z. Y. Xu, Y. J. Gao, X. Yin, Y. H. Hou, L. J. Feng, C. Y. Yue, H. Fei, X. W. Lei, Reversible Triple-Mode Switching in Photoluminescence from 0D Hybrid Antimony Halides, *Chem. Mat.,* 2022, **34(15)**, 6985.
41 T. V. Sedakova, A. G. Mirochnik, Luminescence of Antimony(III) Halogenides Complexes with 2- and 4-Benzylpyridine, *Russ. J. Phys. Chem. A,* 2017, **91(4)**, 791.
42 S. Parmar, S. Pal, A. Biswas, S. Gosavi, S. Chakraborty, M. Chenna Reddy, S. Ogale, Designing a new family of oxonium-cation based structurally diverse organic–inorganic hybrid iodoantimonate crystals, *Chem. Commun.,* 2019, **55(52)**, 7562.
43 L. Romagnoli, A. D'Annibale, E. Blundo, A. Polimeni, A. Cassetta, G. Chita, R. Panetta, A. Ciccioli, A. Latini, Synthesis, Structure, and Characterization of 4,4-(Anthracene-9,10-diylbis(ethyne-2,1-diyl))bis(1-methyl-1-pyridinium) Bismuth Iodide $(C_{30}H_{22}N_2)_3Bi_4I_{18}$, an Air, Water, and Thermally Stable 0D Hybrid Perovskite with High Photoluminescence Efficiency, *Cryst. Growth Des.* 2022, **22(12)**, 7426.
44 E. Suslov, V. V. Zarubaev, A. V. Slita, K. Ponomarev, D. Korchagina, D. M. Ayine-Tora, J. Reynisson, K. Volcho, N. Salakhutdinov, Anti-Influenza Activity of Diazaadamantanes Combined with Monoterpene Moieties, *Bioorg. Med. Chem. Let.,* 2017, **27(19)**, 4531.
45 N. A. Yelovik, A. V. Mironov, M. A. Bykov, A. N. Kuznetsov, A. V. Grigorieva, Z. Wei, E. V. Dikarev, A.V. Shevelkov, Iodobismuthates Containing One-Dimensional BiI_4^- Anions as Prospective Light-Harvesting Materials: Synthesis, Crystal and Electronic Structure, and Optical Properties, *Inorg. Chem.,* 2016, **55(9)**, 4132.
46 Bruker Corporation. SMART (Control) and SAINT (Integration) Software. Bruker AXS Inc.: Madison, WI, USA 1997.
47 L. Krause, R. Herbst-Irmer, G. M. Sheldrick, D. Stalke, Comparison of Silver and Molybdenum Microfocus X-Ray Sources for Single-Crystal Structure Determination, *J. Appl. Cryst.,* 2015, **48(1)**, 3.
48 O. V. Dolomanov, L. J. Bourhis, R. J. Gildea, J. A. K. Howard, H. Puschmann, OLEX2: A Complete Structure Solution, Refinement and Analysis Program, *J. Appl. Cryst.,* 2009, **42(2)**, 339.
49 G. M. Sheldrick, Crystal Structure Refinement with SHELXL, *Acta Cryst. C Struct. Chem.,* 2015, **71(1)**, 3.
50 P. Makuła, M. Pacia, W. Macyk, How to Correctly Determine the Band Gap Energy of Modified Semiconductor Photocatalysts Based on UV–Vis Spectra, *J. Phys. Chem. Lett.,* 2018, **9(23)**, 6814.
51 P. Fedeli, F. Gazza, D. Calestani, P. Ferro, T. Besagni, A. Zappettini, G. Calestani, E. Marchi, P. Ceroni, R. Mosca, Influence of the Synthetic Procedures on the Structural and Optical Properties of Mixed-Halide (Br, I) Perovskite Films, *J. Phys. Chem. C,* 2015, **119(37)**, 21304.

Data availability

CCDC 2346041 (for 1), and 2363792 (for 2) contains the supplementary crystallographic data for this paper. These data can be obtained free of charge from The Cambridge Crystallographic Data Centre via www.ccdc.cam.ac.uk/structures. Thermal analysis data, IR spectra, cations' surrounding (including bond lengths), and luminescence decay fitting parameters for compounds 1 and 2 are given in PDF format.